Original Article

Resolution and Discovery
DOI: 10.1556/2051.2016.00036

IN SITU TRANSMISSION ELECTRON MICROSCOPY OF RESISTIVE SWITCHING IN THIN SILICON OXIDE LAYERS

Martial Duchamp,[1*] Vadim Migunov,[1] Amir H. Tavabi,[1] Adnan Mehonic,[2] Mark Buckwell,[2] Manveer Munde,[2] Anthony J. Kenyon,[2] Rafal E. Dunin-Borkowski,[1]

[1]Ernst Ruska-Centre for Microscopy and Spectroscopy with Electrons and Peter Grünberg Institute, Forschungszentrum Jülich D-52425 Jülich, Germany
[2]Department of Electronic and Electrical Engineering, University College London, Torrington Place, London WC1E 7JE, United Kingdom

Received: 09 June, 2016; Accepted: 06 July, 2016

Silicon oxide-based resistive switching devices show great potential for applications in nonvolatile random access memories. We expose a device to voltages above hard breakdown and show that hard oxide breakdown results in mixing of the SiO_x layer and the TiN lower contact layers. We switch a similar device at sub-breakdown fields *in situ* in the transmission electron microscope (TEM) using a movable probe and study the diffusion mechanism that leads to resistance switching. By recording bright-field (BF) TEM movies while switching the device, we observe the creation of a filament that is correlated with a change in conductivity of the SiO_x layer. We also examine a device prepared on a microfabricated chip and show that variations in electrostatic potential in the SiO_x layer can be recorded using off-axis electron holography as the sample is switched *in situ* in the TEM. Taken together, the visualization of compositional changes in *ex situ* stressed samples and the simultaneous observation of BF TEM contrast variations, a conductivity increase, and a potential drop across the dielectric layer in *in situ* switched devices allow us to conclude that nucleation of the electroforming–switching process starts at the interface between the SiO_x layer and the lower contact.

Keywords: *In situ* TEM electrical biasing, Resistive switching SiO_x

Introduction

Nonvolatile resistive random access memory (RRAM) technologies promise low power consumption, fast switching rates, and integration into current device architectures, which makes them attractive candidates for future memory applications. RRAM technologies are typically based on oxides [1] and rely on the application of an external voltage to switch a thin film between low and high resistance states. In bipolar devices, reset and set operations involve the motion of charged defects or ions, while in unipolar devices, the resetting of devices to a high resistance state is believed to be dominated by thermal processes associated with Joule heating [2, 3]. In some materials, both switching mechanisms may be active [4, 5]. Silicon oxide (SiO_x) is a promising material for resistance switching applications as a result of its compatibility with semiconductor fabrication and its low processing cost. Purely SiO_x-based (metal-free) resistive switches were first reported to undergo only unipolar surface-based switching [6]. However, in more recent studies, switching has been shown to occur in the bulk material rather than at its surface [7] and to show characteristics of both unipolar and bipolar switching [8].

The development of a full understanding of the mechanisms that underpin resistance switching processes is crucial for the optimization of RRAM devices and for developing further applications. The crucial questions that need to be answered are related to how and where conductive filaments form and how they become disconnected during the resetting stage. A small number of reports claim to have observed the physical processes that are associated with resistive processes directly. For example, variations in stoichiometry in a ZnO thin film have been shown to be responsible for increases in conductivity and the formation of Zn-rich filaments [9]. Recent conductive atomic force microscopy results have provided tomographic images of conductive filaments in *ex situ* electroformed SiO_x [10]. In previous transmission electron microscopy (TEM) studies of RRAM devices that had been switched *ex situ* [11, 12], the switched areas needed to be localized prior to the preparation of TEM specimens and great care was needed to avoid artifacts introduced by TEM specimen preparation. Most importantly, only the final states of the switching processes could be observed, making it impossible to follow the growth of conductive filaments or to deduce the nature of the switching mechanisms. Recently, *in situ* switching of RRAM devices in

* Corresponding author: M. Duchamp; E-mail: martial.duchamp@gmail.com

This is an open-access article distributed under the terms of the Creative Commons Attribution License, which permits unrestricted use, distribution, and reproduction in any medium for non-commercial purposes, provided the original author and source are credited.

© 2016 The Author(s)

the TEM has been reported for a limited number of systems, most of which are metal-based. In these studies, filament formation resulted from the diffusion of metallic ions from the active electrode and was relatively easy to observe using conventional TEM techniques [13–16].

Here, we present a study of SiO_x-based RRAM devices that are switched both *ex situ* and *in situ* in the TEM. First, we use conventional TEM to characterize two different devices prior to switching. In order to understand the transformation mechanisms that take place during switching, device A was stressed *ex situ* using a W probe and characterized using scanning (S-)TEM (STEM) combined with energy-dispersive X-ray (EDX) analysis. Second, we used a movable W probe to perform sub-breakdown switching of a device *in situ* in the TEM, in order to observe the diffusion mechanism that leads to the growth and destruction of a conductive filament directly. The switching process was followed using bright-field (BF) TEM imaging, resulting in movies recorded while switching the device *in situ*. Third, we used off-axis electron holography in the TEM, a technique that has previously been used to detect charge density variations at grain boundaries in an HfO_2 memory device [17], to measure local variations in electrostatic potential inside a SiO_x layer during switching *in situ* in the TEM in a device geometry based on micro-electromechanical systems (MEMS) technology.

Results and discussion

BF TEM images of as-deposited SiO_x-based RRAM specimens deposited on TiN (device A) and on crystalline Si (100) (device B) are shown in *Figure 1*(*a–d*), respectively. The images are sensitive to both mass-thickness and diffraction contrast and show that there are no visible crystalline regions in the layer or any visible differences between SiO_x deposited under the same conditions on TiN and Si.

Ex situ voltage (16 V) electrical stress using a W probe was applied to device A, in order to study changes in the SiO_x layer during soft breakdown [18]. *Figure S1* shows a conductive atomic force microcopy (AFM) image of the topography in the device after soft breakdown. *Figure 2a* shows a STEM high-angle annular dark-field image of a stressed region, from which it is clear that the layer has been damaged, resulting in a lifting-up and intermixing of some of the layers. STEM EDX linescans, which are shown in *Figure 2b–d*, were recorded to understand the structural and compositional changes associated with the soft breakdown process. The red arrows in *Figure 2a* indicate regions from which the linescans were acquired. At the tip position, which is assumed to be the region where the greatest damage took place, no Si can be detected. Further from the stressed region (in the area marked “b” in *Figure 2a*), the SiO_x film shows no visible damage, i.e., no intermixing of the layers. *Figure 2c* shows a STEM EDX linescan recorded closer to the stressed area (marked “c” in *Figure 2a*), where Si diffusion into the TiN layer and a corresponding decrease in Ti can be seen. The fact that the layer has been modified at a lateral distance of more than 1 μm from the W probe suggests that there may be a lateral conduction path in the SiO_x layer before it breaks down. Intermixing between SiO_x and TiN is visible in several places between positions “c” and “d” in *Figure 2a*, suggesting the presence of defects in the SiO_x

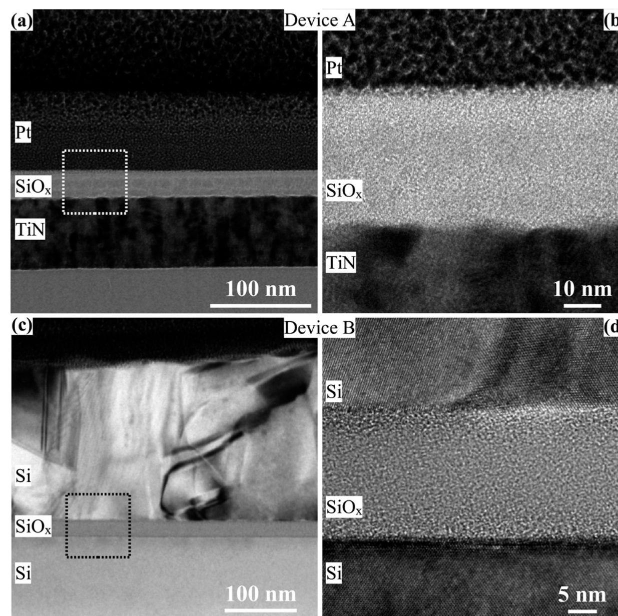

Fig. 1. Bright-field TEM images of SiO_x-based resistive switching memories. The low magnification images in (a) and (c) show (a) the SiO_x layer deposited on TiN (device A) and (c) the SiO_x layer embedded between single crystalline Si and polycrystalline Si (device B). The corresponding high-resolution TEM images in (b) and (d) do not show any visible nanocrystals in the SiO_x layer. The boxes in (a) and (c) indicate the positions of the regions in images (b) and (d), respectively

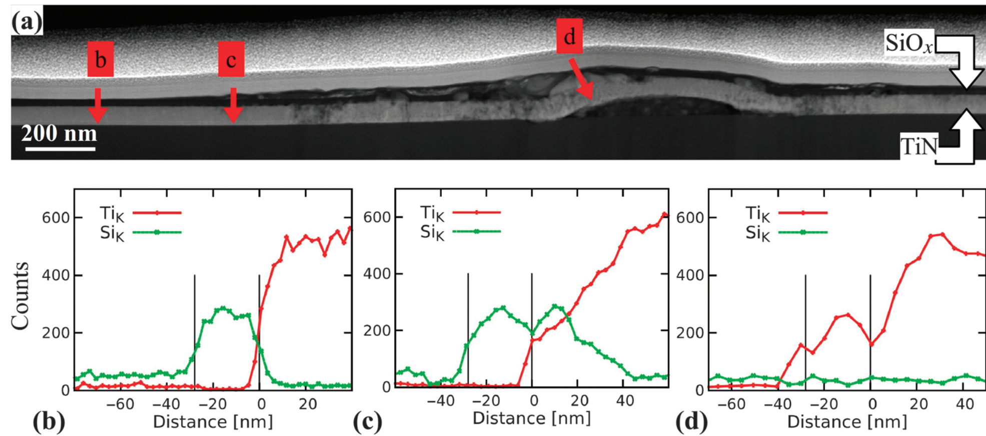

Fig. 2. (a) STEM HAADF image showing structural damage in the TiN and SiO_x layers in device A after over-stressing the specimen *ex situ*. (b–d) Single-pixel STEM EDX linescans recorded along the lines marked using solid red arrows in (a). The directions of the arrows correspond to left to right directions in each linescan. The vertical black lines in (b–d) are the estimated positions of the original boundaries of the SiO_x layer

layer before stressing. The voltage applied during soft breakdown is slightly higher than voltages used under normal working conditions. This was necessary in order to overcome the additional tunneling barrier present on the SiO_x surface as a result of native oxidation [18].

In situ sub-breakdown TEM switching of device A using a movable W probe was performed in order to study the details of the switching process. Switching was performed by sweeping the voltage first in the positive direction (from 0 to 14 V) and then in the negative direction (from 14 to 0 V). The applied voltages are higher in devices with top electrodes as a result of the relatively high contact resistance between the probe and the oxide layer. During *in situ* switching in the TEM, the positive direction of the applied electric field is from the W tip to the TiN layer. The current I and BF TEM images were recorded while varying the applied voltage V. A representative I–V curve is shown in *Figure 3b*. The current is higher in the downward voltage sweep than in the upward sweep, suggesting resistance switching during the upward sweep. The voltage was limited during the experiment to avoid overloading the device and consequent hard breakdown. Currents below 1 nA were measured for applied voltages below 5 V, indicating that the dielectric layer is highly resistive. A sudden increase in current at ~10 V is associated with structural modifications, which can be seen in *Figure 3c–e* in the form of frames extracted from a movie of BF TEM images (the full movie is in Supporting Information). The green arrow shows a crystal of TiN, which serves as a reference point to locate the area of interest. The red arrows mark regions in the SiO_x layer that have darker contrast and evolve with applied voltage. Above 10 V, the dark areas grow continuously with increasing voltage, extending from the bottom contact to the W probe at ~12 V. At this voltage, a continuous region of dark contrast is observed across the SiO_x layer in the corresponding TEM image (*Figure 3e*). For higher voltages, a smaller region of dark contrast, which has narrowed in the direction of the layer, extends up to the TiN–SiO_x interface (*Figure 3f*). When decreasing the applied voltage (*Figure 3f–h*), the reverse process is observed, i.e., the dark areas shrink (full movie in Supporting Information). In order to obtain a better understanding of resistive switching phenomena, it would be important to measure the relationship between the volume of the dark contrast and the conductivity. However, the required depth information in the electron beam direction is not available at present. The advent of fast 3D tomography [19] promises to allow three-dimensional information about such conductive channels to be revealed. Interestingly, even for voltages below 5 V, when a negligible current is measured, a remaining area of dark contrast is present at the TiN–SiO_x interface, suggesting that part of the SiO_x layer remains conducting in the absence of an applied voltage. We expect that such regions may be more extensive if a higher voltage is applied during switching. The fact that growth of the area of dark contrast is from the TiN to the tip suggests either that positive ions move toward the W tip [20] or that negative ions move toward the TiN bottom contact. Moreover, we do not observe any effect on the TiN layer during the switching process. Darker contrast visible in the BF TEM imaging mode originates either from a thicker sample or from a higher mass density compared to the surrounding SiO_x. In order to investigate the origin of the dark contrast more deeply, similar experiments were performed using dark field (DF) TEM (*Figure S4a*) and HAADF STEM (*Figure S4b*). The I–V curves recorded under these different imaging conditions are similar to that recorded under BF TEM imaging, demonstrating good reproducibility of *in situ* TEM switching. No contrast variations were observed under dark-field imaging conditions, ruling out local changes in the crystalline nature of the sample. Similarly, no contrast variations were observed under HAADF STEM imaging conditions, ruling out significant local variations in the migration of Ti. EDX spectroscopy was used to look for variations in composition after *in situ* switching. No local variations in Si or Ti were detected at the positions of the remaining dark contrast after *in situ* switching by performing EDX (*Figure S5*). It is also interesting to observe that, in both

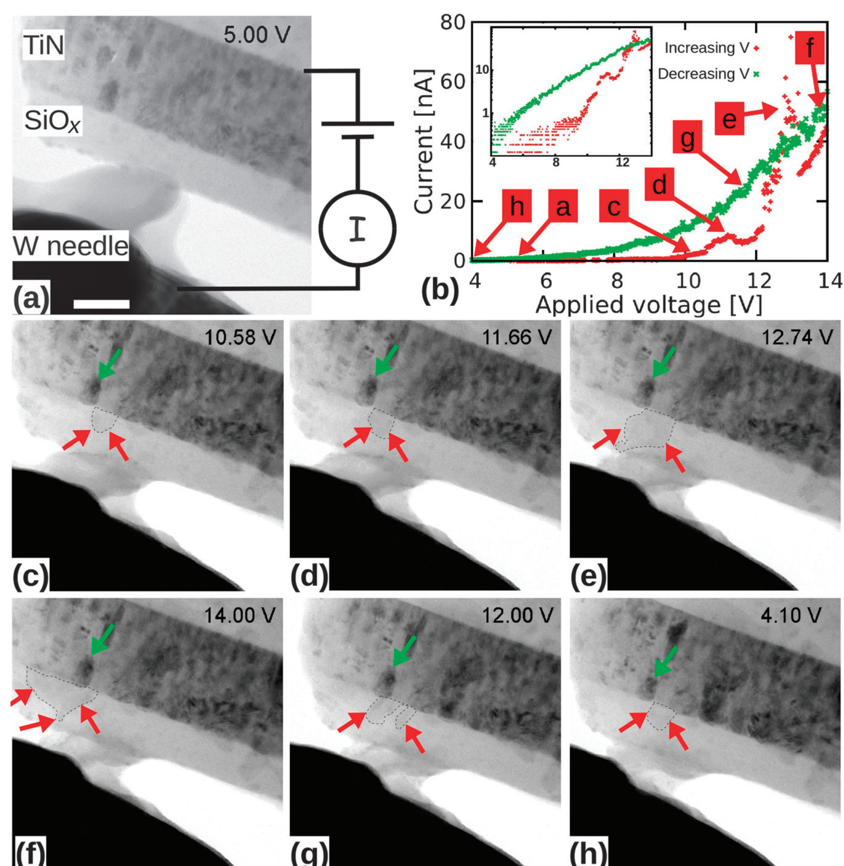

Fig. 3. *In situ* observation of the formation of a conductive path in the SiO_x layer in device A recorded while using a movable W needle in a Nanofactory specimen holder to apply a bias locally to the specimen in the TEM. (a) Bright-field TEM image of the device recorded during the application of an initial 5 V bias, showing no visible change from the as-fabricated device. A schematic diagram of the electrical setup used during the *in situ* TEM experiment is shown on the right of the image. (b) Current–voltage (*I*–*V*) measurements recorded while performing *in situ* switching of the device using a W probe in the TEM. The red and green dots correspond to positive and negative voltage sweeps, respectively. The letters in the red boxes correspond to TEM images (c–h). The insert shows the same plot displayed in the form of *I*–log(*V*). Images (c–e) were recorded while increasing the voltage, while images (f–h) were recorded while decreasing the voltage. The red arrows in (c–h) indicate the part of the SiO_x layer that changes during the sweep. The green arrow indicates a crystal in the TiN layer that can be used as reference point during the switching process. The dashed lines in (c–h) mark the regions of dark contrast resulting from the applied voltage. The scale bar in (a) is 30 nm. The full bright-field TEM movie of the *in situ* switching experiment is available in Supplementary Information

the *in situ* and the *ex situ* experiments, the origin of the migration process takes place at the SiO_x–TiN interface.

In situ switching and electron holographic TEM was performed on device B, which was mounted on a MEMS chip. In the previous experiments, switching was performed using a movable W probe, either *ex situ* or *in situ* in the TEM, in order to allow the switched area to be identified. In both cases, the top contact was missing and the W tip was in direct contact with the SiO_x layer. A full device was therefore not probed. In a real device, the location of the region that switches in the SiO_x layer, which is sandwiched between the top and bottom contacts, is usually unknown. Moreover, the switching mechanism may not be homogeneous across the layer, as indicated by the non-uniformity of defects after *ex situ* soft breakdown of the sample (*Figure 2*). Thus, the voltage applied with a ~20 nm W tip to a specific region may not be representative of that in a complete device. We therefore prepared a TEM lamella for *in situ* switching of a complete device (i.e., with both the top and the bottom electrode present), as shown in *Figure 4a*. The specimen was prepared from device B, in which the SiO_x layer is deposited on a Si substrate. A representative *I*–*V* curve measured from this device *in situ* in the TEM is shown in *Figure 4b*. Voltages of between −20 and +30 V were applied to the device *in situ* in the TEM. For voltages above 20 V, the current through the specimen reached the chosen compliance value of 10 nA (for higher voltages, the applied voltage is automatically adjusted to match the current compliance and the device resistance). Off-axis electron holograms were recorded while applying voltages to the device. The technique allows the measurement of variations in both the applied electrostatic potential and the mean inner potential (MIP), which is strongly sensitive to structural changes in the specimen. Phase images recorded for applied voltages of 0, 20, and 25 V are shown in *Figure S3*. The images for 0 and 25 V are similar to each other but different to that for 20 V, indicating that an additional voltage is present at 20 V but not at 25 V (at this voltage, the current compliance was reached, and the applied voltage was reduced to

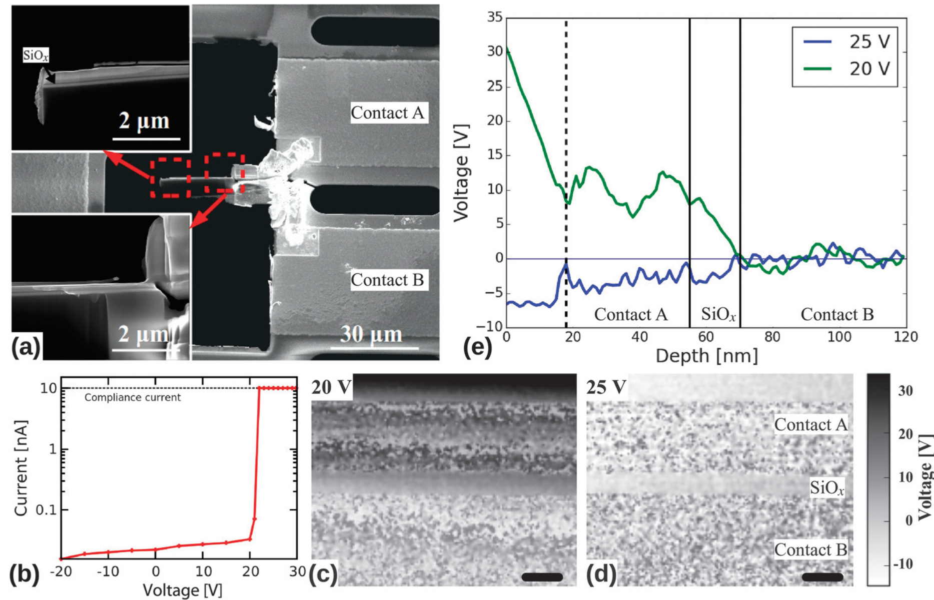

Fig. 4. (a) Secondary electron image recorded in a scanning electron microscope from the central part of a MEMS chip, onto which a TEM specimen of device B has been attached and contacted electrically in a FIB workstation. The top polycrystalline Si layer and the Si wafer are connected to contacts A and B using ion-beam-deposited Pt so that the SiO_x layer can be biased electrically *in situ* in the TEM. Contact B was kept at ground potential, and chosen voltages were applied to contact A. The insets show higher magnification scanning electron micrographs of the layers of interest and the electrical contacts to the device. (b) *I–V* curve measured from the device in (a), showing a linear increase in current with applied voltage up to 20 V, followed by an abrupt increase in current, corresponding to a transition from the "off" to the "on" state of the device measured *in situ* in the TEM. The measurements were obtained while recording electron holograms. (c) and (d) show phase difference images between the unbiased state (0 V) and states recorded with (d) 20 and (e) 25 V applied to the specimen. Phase unwrapping was performed on each original phase image inside the SiO_x layer, while phase wraps were retained in the much noisier regions corresponding to the electrical contacts. The final phase difference images were converted to the indicated voltage scale on the assumptions that the electrically active specimen thickness is 50 nm, that the voltage is contained with the specimen, and that it is uniform in the electron beam direction. The phase difference images do not show the presence of conductive paths in the "off" or "on" states of the device. The scale bars in (c) and (d) are 20 nm. (e) Line profiles generated by averaging the difference images in (c) and (d) horizontally. On the assumption that the electrically active specimen thickness is 50 nm, a potential drop of 10 V is measured across the SiO_x layer when 20 V is applied to the device. See text for discussion and further details. The slope on the left side of the 20 V line profile is likely to arise from an electrostatic fringing field in vacuum outside the edge of the TEM specimen

match the specimen resistance). In *Figure S3*, both the MIP contribution to the phase and the contribution to the phase from the applied voltage are still present, resulting in a variation in contrast in the dielectric layer that is likely to be dominated by specimen thickness variations. Differences between phase images recorded with no applied voltage and phase images recorded for applied voltages of 20 V and 25 V are therefore shown in *Figure 4c* and *d*, respectively. The images show that a voltage is dropped across the SiO_x layer at 20 V but not at 25 V. *Figure 4e* shows line profiles of the phase difference images averaged perpendicular to the SiO_x layer growth direction. On the assumption of an electrically active layer thickness of 50 nm (in the electron beam direction), the measured phase shift corresponds to a 10-V drop across the SiO_x layer. No significant nanometer-scale local changes in MIP are visible in the oxide layer in the phase difference images, even though the conductivity of the SiO_x changed between the "off" and the "on" state of the device and more than 90% of the specimen was visible during the experiment.

We have used a wide range of TEM techniques to study changes in chemical composition when applying voltages to a SiO_x layer in a RRAM device. STEM EDX and BF TEM imaging were applied during both hard and soft breakdown in specimens that had been switched both *ex situ* and *in situ* in the TEM. The formation and disappearance of a conductive filament was observed during switching *in situ* in the TEM using a movable W probe. In both the *ex situ* and the *in situ* experiments, the migration process was observed to take place at the SiO_x–TiN interface. Off-axis electron holography was used to measure the electrostatic potential inside the SiO_x layer in a real device, in which the conductivity increases during a voltage ramp. The device geometry that we describe is promising for future *in situ* studies when simultaneous electrical and structural modifications under an applied electrical bias are expected and can be combined with an external temperature stimulus.

Methods

Device fabrication and ex situ switching

Resistance switching device structures containing thin (40 nm) SiO_x layers were grown both on TiN without a top contact (device A) and between a *p*-type Si substrate

and an *n*-type poly-silicon contact (device B). We have previously studied devices A biased with tungsten probes and have established that the resistance changes, and hence, structural modifications, are essentially the same as in devices B with a top contact [21]. Further details about the fabrication process can be found in Refs. 7 and 20. Device A was electrically formed by using a W probe to switch the sample on a contact-free area. A conductive spot was formed directly on the SiO_x layer with an applied voltage of 16 V and a 100-μA current compliance using a nominally 1 μm diameter W probe from a Keithley 4200 semiconductor characterization system. Device A was imaged using a Bruker Icon microscope with Pt/Ir-coated Si cantilevers using a nominal tip diameter of 20 nm (*Figure S1*). The region was scanned with 10 V applied to the bottom electrode, and the tip was grounded. This voltage was required to record a measurable current due to the tunneling gap between the tip and the sample, as scanning did not involve pressing hard into the surface. The compliance current of the microscope was 500 nA.

Cross-sectional TEM specimens of device A were prepared using a standard lift-out procedure in an FEI Helios dual-beam focused ion beam (FIB) workstation. *In situ* switching of device A in the TEM was performed using a Nanofactory TEM specimen holder. The experiments involved coating the SiO_x with a layer of ink, followed by electron-beam-deposited Pt and ion-beam-deposited Pt in the FIB workstation. Coarse FIB milling was carried out using a 30-kV ion beam, with final milling performed at 5 kV. Removal of the outermost damaged layers after FIB milling was performed using a 900-V focused Ar beam in a Fischione Instruments Nanomill 1040 workstation. The ink and Pt layers were then detached from the lamella to expose the SiO_x for electrical contacting inside the TEM using the manipulator of the Nanofactory specimen holder (*Figure S2*).

For *in situ* switching of device B, specimens were prepared in the form of MEMS chips and contacted electrically using FIB and a lift-out procedure, as described in detail elsewhere [22, 23]. The procedure, which has been used for the preparation of high quality specimens for *in situ* annealing [22] and biasing [23], involves initially transferring a thick (~3 μm) TEM lamella from a bulk sample to a MEMS chip. Electrical contacts are then added using ion-beam-deposited Pt. The final step consists of thinning the thick lamella directly on the MEMS chip, thereby preventing unwanted Ga implantation and Pt redeposition during the transfer and contacting steps and allowing both backside and frontside milling.

TEM set-ups

High-angle annular dark-field (HAADF) STEM experiments were carried out in an FEI Tecnai G20 TEM operated at 200 kV using a convergence semi-angle of ~15 mrad and an inner collection semi-angle of ~70 mrad to provide atomic-number-sensitive contrast. STEM EDX linescans were acquired using an EDAX Si(Li) detector with an acquisition time of 1 s/pixel at 10 eV/channel. *In situ* switching experiments were performed at 300 kV in an FEI Titan TEM equipped with an image CS corrector and two electron biprisms. Switching of device A was performed using a scanning tunneling microscopy TEM specimen holder (Nanofactory Instruments AB, Göteborg, Sweden) equipped with a movable W probe. Switching of device B was performed using a DENSSolutions double tilt four contact MEMS TEM specimen holder.

In situ off-axis electron holography

In order to monitor changes in both mean inner potential and applied electrostatic potential, device B was studied using off-axis electron holography. The technique allows both the amplitude and the phase shift of the electron wave that has passed through a specimen to be recorded in the TEM. The phase shift is proportional to the electrostatic potential in the specimen projected in the electron beam direction. The potential can be described in terms of a sum of the mean inner potential and additional potentials such as those associated with applied voltages, built-in potentials, or electrical charging of the specimen. In the absence of magnetic fields and diffraction contrast, the phase shift of the electron wave (compared to a reference wave traveling in a field-free vacuum region) is given by the expression

$$\varphi(x,y) = C_{\mathrm{E}} \int_{z=-\infty}^{z=+\infty} V(x,y,z)dz \,, \qquad (1)$$

where C_{E} is a constant that depends on the electron microscope accelerating voltage, z is the incident electron beam direction, and V is the total electrostatic potential (including the mean inner potential). In a specimen of uniform thickness, in the absence of electrostatic fringing fields, the measured phase is directly proportional to the potential averaged through the thickness of the specimen. In order to subtract the mean inner potential contribution from the recorded signal, differences between phase images recorded with different voltages applied across the SiO_x layer were evaluated, as reported elsewhere [24].

Acknowledgements

The authors acknowledge financial support from the European Union under the Seventh Framework Programme under a contract for an Integrated Infrastructure Initiative (Reference 312483 — ESTEEM2) and are grateful to Prof. Michael Farle of the University of Duisburg-Essen for valuable technical assistance.

Author contributions

MD, VM, and AT designed and conducted the *in situ* TEM experiments. AM, MB, and MM prepared the

RRAM devices and performed *ex situ* switching experiments. MD wrote the article, with contributions from all of the other authors. All of the authors discussed the results and commented on the article.

Supporting information

Electronic Supplementary Material (ESM) accompanies this paper at doi: 10.1556/2051.2016.00036.

References

1. Saleh MN, Venkatachalam DK, Elliman RG: Effect of crystallization on the reliability of unipolar resistive-switching in HfO_2-based dielectrics. Curr Appl Phys 14, S88–S92 (2014)
2. Waser R, Dittmann R, Staikov G, Szot K: Redox-based resistive switching memories — nanoionic mechanisms, prospects, and challenges. Adv Mater 21, 2632–2663 (2009)
3. Strukov DB, Alibart F, Williams RS: Thermophoresis/diffusion as a plausible mechanism for unipolar resistive switching in metal–oxide–metal memristors. Appl Phys A 107, 509–518 (2012)
4. Jeong DS, Schroeder H, Waser R: Coexistence of bipolar and unipolar resistive switching behaviors in a Pt/TiO_2/Pt stack. Electrochem Solid-State Lett 10, G51–G53 (2007)
5. Schindler C, Thermadam SCP, Waser R, Kozicki MN: Bipolar and unipolar resistive switching in Cu-doped SiO_2. IEEE Trans Electron Devices 54, 2762–2768 (2007)
6. Yao J, Sun Z, Zhong L, Natelson D, Tour JM: Resistive switches and memories from silicon oxide. Nano Lett 10, 4105–4110 (2010)
7. Mehonic A, Cueff S, Wojdak M, Hudziak S, Jambois O, Labbé C, Garrido B, Rizk R, Kenyon AJ: Resistive switching in silicon suboxide films, J. Appl. Phys. 111, 74507 (2012)
8. Mehonic A, Cueff S, Wojdak M, Hudziak S, Labbé C, Rizk R, Kenyon AJ: Electrically tailored resistance switching in silicon oxide, Nanotechnology. 23, 455201 (2012)
9. Chen J-Y, Hsin C-L, Huang C-W, Chiu C-H, Huang Y-T, Lin S-J, Wu W-W, Chen L-J: Chen, Dynamic Evolution of Conducting Nanofilament in Resistive Switching Memories, Nano Lett. 13, 3671 (2013)
10. Buckwell M, Montesi L, Hudziak S, Mehonic A, Kenyon AJ: Conductance tomography of conductive filaments in intrinsic silicon-rich silica RRAM. Nanoscale 7, 18030 (2015)
11. Privitera S, Bersuker G, Butcher B, Kalantarian A, Lombardo S, Bongiorno C, Geer R, Gilmer DC, Kirsch PD: Microscopy study of the conductive filament in HfO_2 resistive switching memory devices, Microelectron. Eng. 109, 75 (2013)
12. Lee D, Sung Y, Lee I, Kim J, Sohn H, Ko D-H: Enhanced bipolar resistive switching of HfO_2 with a Ti interlayer, Appl. Phys. A. 102, 997 (2011)
13. Kamaladasa RJ, Sharma AA, Lai Y-T, Chen W, Salvador PA, Bain JA, Skowronski M, Picard YN: *In situ* TEM Imaging of Defect Dynamics under Electrical Bias in Resistive Switching Rutile-TiO_2, Microsc. Microanal. 21, 140 (2015)
14. Yang Y, Gao P, Gaba S, Chang T, Pan X, Lu W: Observation of conducting filament growth in nanoscale resistive memories, Nat. Commun. 3, 732 (2012)
15. Fujii T, Arita M, Takahashi Y, Fujiwara I: *In situ* transmission electron microscopy analysis of conductive filament during solid electrolyte resistance switching. Appl Phys Lett 98, 212104 (2011)
16. Tian X, Yang S, Zeng M, Wang L, Wei J, Xu Z, Wang W, Bai X: Bipolar Electrochemical Mechanism for Mass Transfer in Nanoionic Resistive Memories, Adv. Mater. 26, 3649 (2014)
17. Yao J, Sun Z, Zhong L, Natelson D, Tour JM: Resistive Switches and Memories from Silicon Oxide, Nat Comm 4, 2764 (2013)
18. Buckwell M, Montesi L, Mehonic A, Reza O, Garnett L, Munde M, Hudziak S, Kenyon AJ: Microscopic and spectroscopic analysis of the nature of conductivity changes during resistive switching in silicon-rich silicon oxide, Phys. Status Solidi C. 12, 211 (2015)
19. Migunov V, Ryll H, Zhuge X, Simson M, Strüder L, Batenburg KJ, Houben L, Dunin-Borkowski RE: Rapid low dose electron tomography using a direct electron detection camera, Sci. Rep. 5, 14516 (2015)
20. Wedig A, Luebben M, Cho D-Y, Moors M, Skaja K, Rana V, Hasegawa T, Adepalli KK, Yildiz B, Waser R, Valov I: Nanoscale cation motion in TaO_x, HfO_x and TiO_x memristive systems. Nat Nanotechnol 11, 67 (2015)
21. Mehonic A, Buckwell M, Montesi L, Garnett L, Hudziak S, Fearn S, Chater R, McPhail D, Kenyon AJ: Structural changes and conductance thresholds in metal-free intrinsic SiO_x resistive random access memory. J Appl Phys 117, 124505 (2015)
22. Duchamp M, den Hertog M, Imlau R, Boothroyd CB, Kovacs A, Tavabi AH, Dunin-Borkowski RE: Focused ion beam specimen preparation for electron holography of electrically biased thin film solar cells, in: Rachel R (Ed.), Microsc. Conf. MC2013 Regensbg. Ger. 25-30 August 2013, Regensburg, 2013: pp. 242–243. http://epub.uniregensburg.de/28734/1/MC2013_Proceedings_Part_I.pdf.
23. Duchamp M, Xu Q, Dunin-Borkowski RE: Convenient Preparation of High-Quality Specimens for Annealing Experiments in the Transmission Electron Microscope, Microsc. Microanal. 20, 1638 (2014)
24. Migunov V, London A, Farle M, Dunin-Borkowski RE: Model-independent measurement of the charge density distribution along an Fe atom probe needle using off-axis electron holography without mean inner potential effects. J. Appl. Phys. 117, 134301 (2015)